ENHANCEMENT OF FRACTURE RESISTANCE BY MULTIPLE CRACKS IN LAYERED STRUCTURES UNDER MODE I AND MIX MODE LOADING

Stergios Goutianos and Bent F. Sørensen

Department of Wind Energy, Section of Composites and Materials Mechanics,
Technical University of Denmark, Risø Campus, DK-4000 Roskilde, Denmark

Keywords: Fracture resistance, Delamination, Cohesive law, Multiple cracks

ABSTRACT

Model results show that the fracture resistance of a layered structure can be significantly enhanced by introducing weak layers next to a damage prone area. The fracture resistance increase is due to simultaneous multiple cracks/delaminations. Cohesive zone modelling is being used to verify analytical predictions under pure mode I and mix mode loading. It is shown that for a wide range of cohesive law parameters, numerical predictions agree well quantitatively with the theoretical model. The most important parameters controlling whether a secondary crack forms is the peak cohesive traction value and the ply thickness. Thus, it can be argued that it is possible to enhance the fracture resistance of a structure considerably by controlling interfaces and create weak layers.

1 INTRODUCTION

Layered structures are susceptible to delamination because they often exhibit low interlaminar fracture resistance. Through-thickness stresses e.g. due to manufacturing defects or geometric discontinuities, can result in initiation and growth of interlaminar cracks which may lead to loss of structural integrity [1,2]. A number of techniques have been developed to increase the through-thickness fracture resistance of layered structures e.g. fibre reinforced composites. In composite materials, two routes to develop damage tolerant composites have been followed: a) tougher matrices [3] and inclusion of interleaves [4] and b) modifications of the fibre architecture e.g. stitching [5], z-pinning [6], knitting [7] and braiding [8]. These techniques aim to increase the fracture resistance by making the damage prone areas stronger.

In the present work, an alternative approach is followed. We explore the possibility of increasing the fracture resistance of a layered structure by introducing weak planes that result in multiple delaminations next to a damage prone area. The idea is shown schematically in Fig. 1.

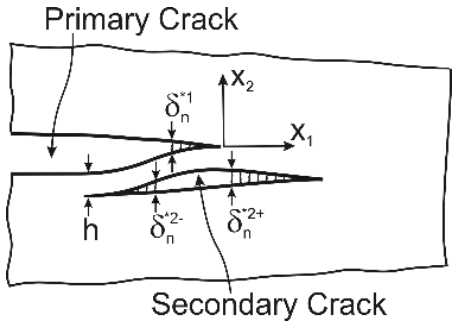

Figure 1: Crack in a weak layer (secondary crack) as a distance *h* from the primary crack. δ_n^{*1} is the normal end-opening of the primary crack. δ_n^{*2-} and δ_n^{*2+} are the normal end-openings of the right and left hand side crack tips of the secondary crack.

The approach is motivated by the experimental results of Rask and Sørensen [9] who observed that by changing the ply thicknesses of composite beams bonded together with a thermoset adhesive, more

delamination cracks could be developed next to the original adhesive/laminate crack. They found that the overall steady-state fracture resistance increases proportionally with the number of secondary cracks suggesting a linear relationship between the number of cracks/fracture process zones and the overall steady-state fracture resistance.

Since crack growth/delamination in fibre composite materials [10] or in adhesive joints between composite materials [11] involves large scale fibre bridging, the analytical model is based on the path independent *J* integral [12] and thus it is valid for large-scale fracture process zones.

To test the analytical predictions, a numerical model (cohesive zone modelling implemented in a finite element framework, valid also for large-scale fracture process zones) is used. The finite element problem analysed is a DCB specimen subjected to pure bending moments as shown in Fig. 2. In order to keep the model simple, only two delamination planes, a primary and a secondary crack plane are defined.

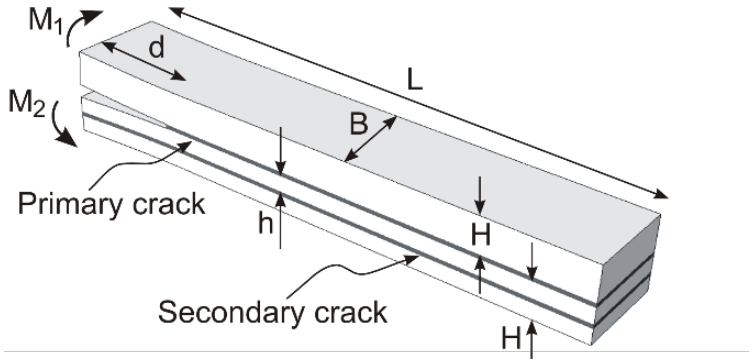

Figure 2: Double Cantilever Beam (DCB) specimen subjected to pure bending moments M_1 and M_2. A notch of length *d* is used to initiate the primary crack. A second, potential, crack is defined at a distance *h* from the primary crack.

2 ANALYSIS

The mechanism of the simultaneous crack growth of the primary and secondary crack of Fig. 2, is analysed in this Section.

2.1 Concept of cohesive laws

The fracture process zone of both the primary and secondary crack can be modelled by a cohesive zone model [13,14]. The tractions across the crack faces of the fracture process zone are described by cohesive laws or traction-separation laws shown in Fig. 3 for pure mode I and mode II (*i*=1 for the primary crack and *i*=2 for the secondary crack).

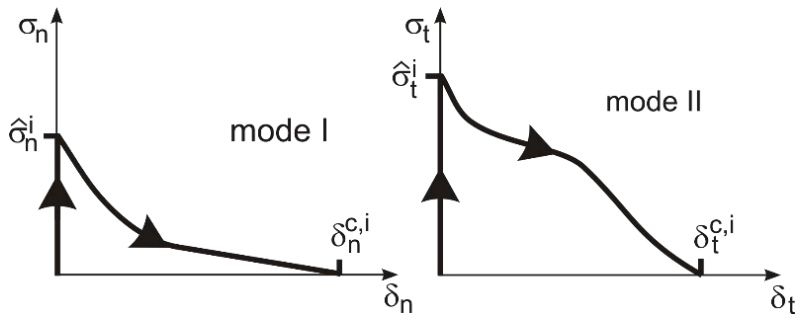

Figure 3: Schematic of cohesive laws. $\hat{\sigma}_n^i$ and $\hat{\sigma}_t^i$ are the normal and shear peak tractions. δ_n^i and δ_t^i are the normal and shear openings (*i*=1 for the primary crack and *i*=2 for the secondary crack).

2.2 Description of multiple crack initiation and growth

In the description of multiple cracks formation, we consider the case of pure mode I loading ($M_1 = -M_2$ in Fig. 2). Under monotonically increasing applied load, the normal traction ahead of the notch increases continuously. When the normal stress at the primary crack tip reaches $\hat{\sigma}_n^1$, the crack starts to open. If at distance *h*, where the weak plane lies (the second cohesive zone), the normal stress is less than $\hat{\sigma}_n^2$ at any material point along the plane, then there is no crack formation in this plane.

As the primary crack grows with increasing applied load, the tractions next to the primary crack increase. If the normal stress at the secondary plane reaches the peak traction $\hat{\sigma}_n^2$, then the secondary crack forms, close to the current tip of the primary crack. Upon further increase of the applied load, both cracks grow (at a different rate) and eventually they are fully developed. The work per unit area behind the primary crack tip is denoted as J_{ss}^1 , for the secondary crack as J_{ss}^2, and for the combined work (overall steady-state fracture resistance) as $J_{R,ss}$.

2.3 *J* integral analysis

The path independent J integral [12] can be used to derive the overall fracture resistance of the problem shown in Fig. 1. Using a local integration path just outside the cracks (fracture process zones), it can be shown that the local *J* integral is [15]:

$$J_{loc} = J_{loc}^1 + J_{loc}^{2-} + J_{loc}^{2+} \tag{1}$$

where J_{loc}^1 is the *J* integral value for the path around the primary crack. J_{loc}^{2-} and J_{loc}^{2+} are the *J* integral values for the parts of the path running along the crack faces of the left and right hand side of the secondary crack, respectively. If the secondary crack extends in both direction then [15]:

$$J_{loc} = J_{loc}^1 \tag{2}$$

whereas if the left hand side crack tip of the secondary crack remains closed then [15]:

$$J_{loc} = J_{loc}^1 + J_{loc}^{2+} = \Gamma_n^1 + \Gamma_n^2 \tag{3}$$

The right hand side crack tip of the secondary crack provides a direct contribution to the overall fracture resistance (from path independence $J_{R,ss} = J_{ext} = J_{loc}$). $\boldsymbol{\Gamma_n^1}$ and $\boldsymbol{\Gamma_n^2}$ are the mode I and mode II fracture energy for the primary and secondary crack, respectively and represent the total area under the cohesive laws for each mode. Eq. 2 can be generalised to *N* secondary (delamination) cracks and to mix mode loading:

$$J_{R,ss} = J_{loc} = J_{loc}^1 + J_{loc}^{2+} = \Gamma_\phi^1 + N\,\Gamma_\phi^2 \tag{4}$$

where Γ_ϕ^1 and Γ_ϕ^2 are the fracture energies (functions phase angle of openings ϕ) of the primary and secondary cracks.

3 NUMERICAL MODEL

3.1 Finite element model

The crack growth problem of Fig. 2 was modelled as a plane strain problem as shown in Fig. 4. Pure bending moments are applied to the left hand side beams through rotational displacements in two points tied to two analytical rigid surfaces tied to the beams.

An explicit solver (Abaqus) was used under quasi-static conditions using mass-scaling. It was ensured that the sum of the kinetic energy and the energy dissipated by viscosity (viscous damping) was less than 0.5% of the strain energy.

The *J* integral evaluated along the external boundaries, under plane strain and mixed mode loading is [16]:

$$\boldsymbol{J_{ext} = (1-\nu)^2 \, \frac{21\left(M_1^2 + M_2^2\right) - 6M_1M_2}{4B^2H^3E}} \tag{5}$$

where *H* and *B* are shown in Fig. 2. *E* and ν are the Young's modulus and Poisson's ratio of the beams and the moments M_1 and M_2 applied to the left hand beam ends are taken positive in the same direction. The J integral result is independent of the crack lengths and therefore the overall fracture resistance can be directly calculated by extracting the moments from the finite element solutions.

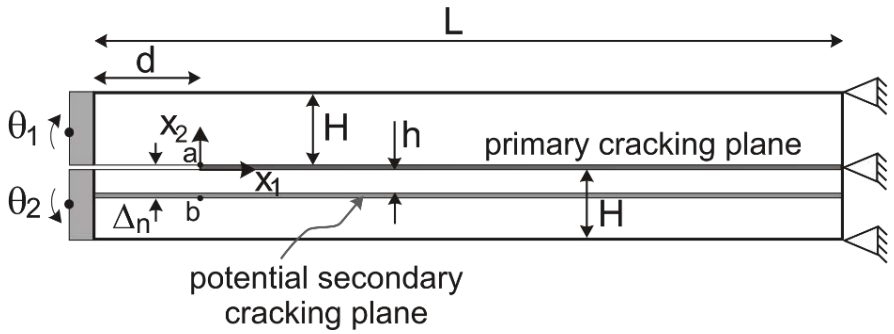

Figure 4: Geometry, boundary conditions and loads of the finite element model. The primary crack plane and the potential crack plane are shown.

3.2 Cohesive zone modelling

The crack planes for the primary and potential secondary crack plane are modelled with cohesive elements of finite thickness (0.01*H*) to avoid interpenetration of the surfaces adjacent to the cohesive elements. The cohesive zone of the secondary crack extends along the entire specimen length, allowing crack extension behind the initial notch.

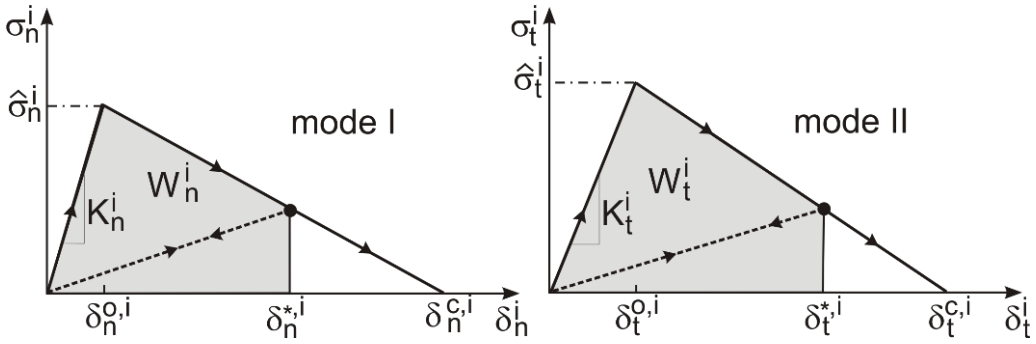

Figure 5: Mode I and mode II bilinear cohesive laws for the primary (*i*=1) and secondary crack (*i*=2).

The cohesive laws have a bilinear shape as shown in Fig. 5. The cohesive law stiffnesses, K_n^i and K_t^i for the primary and secondary cracks are assigned high values to practically have linear softening cohesive laws with minimum opening prior to crack opening. It is assumed that the normal and shear laws are independent from each other but coupled through a simple failure criterion [17,18]:

$$\boldsymbol{F_{crit} = \frac{W_n^i}{\Gamma_n^i} + \frac{W_t^i}{\Gamma_t^i} = 1, \quad i = 1 \; or \; 2} \tag{6}$$

where W_n^i and W_t^i (shaded areas in Fig. 5) represent the work of the normal and shear cohesive tractions, respectively.

The cohesive laws were implemented in a user-defined Abaqus material subroutine. Since in the analytical model it is assumed that the left hand side of the secondary crack can unload, it is important to include unloading in the implementation of the cohesive laws. The unloading behaviour is show with dotted lines in Fig. 5

4 RESULTS

The overall steady-state fracture resistance depends on a large number of parameters such as the cohesive law properties of the secondary crack and the cohesive law properties of the primary crack. The mode II cohesive law properties with respect to the mode I cohesive law both for the primary and secondary crack. Except from the material properties, geometry, distance *h*, affects the enhancement of the steady-state fracture resistance. Thus, only few selected results are shown in the present work.

4.1 Mode I

Fig. 6 shows the overall steady-state fracture resistance increase for different peak tractions of the secondary crack placed at various distances, *h*, from the primary crack. For the results shown in Fig. 6, the mode I and mode II cohesive laws are identical for both cracks. It can be seen that the steady-state fracture resistance is within the limits set by the analytical model (Eqs. 2 and 3). When *h* is small, then $J_{R,ss}$ approaches the upper limit (Eq. 3) for a wide range of $\hat{\sigma}_n^2/\hat{\sigma}_n^1$.

When the peak traction of the secondary crack is larger than the peak traction of the primary crack, then only the primary crack opens/grows and thus there is no enhancement in the overall fracture resistance.

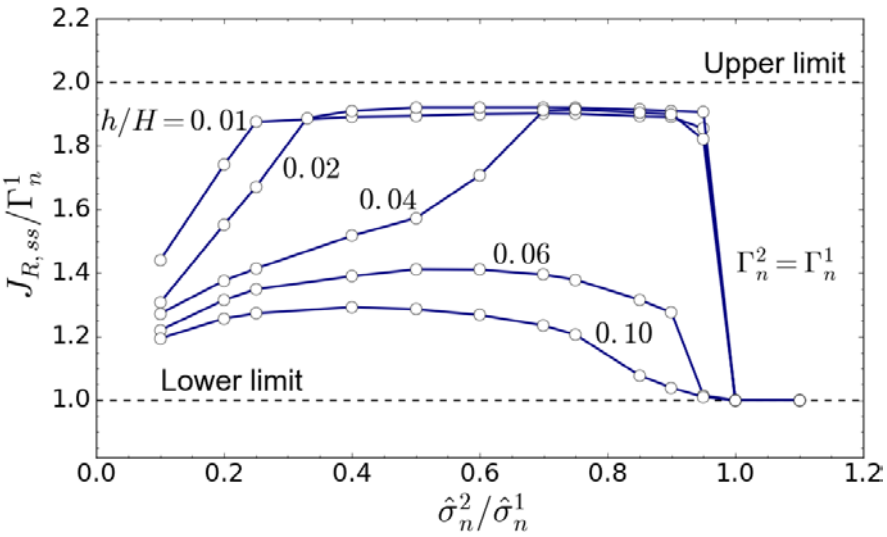

Figure 6: Overall steady-state fracture resistance, $J_{R,ss}$, as a function of the normal peak traction of the secondary crack located at distance *h* from the primary crack. The mode II cohesive law is identical to the mode I cohesive law for the primary crack and for the secondary crack.

4.2 Mix mode

The effect of the mix mode loading in the increase of the steady-state fracture resistance is shown in Fig. 7. In these simulations, the mode I fracture energy is equal to the mode II fracture energy for both cracks. The fracture energy is the same for the primary and secondary crack. When the peak traction of the secondary crack is smaller than the primary crack peak traction, then there is an enhancement of the steady-state fracture resistance for all mode mixities. The effect is more pronounced when the mode mixity is closer to mode I. On the other hand when the mode mixity is large (e.g. 75°), the enhancement

of $J_{R,ss}$ is moderate.

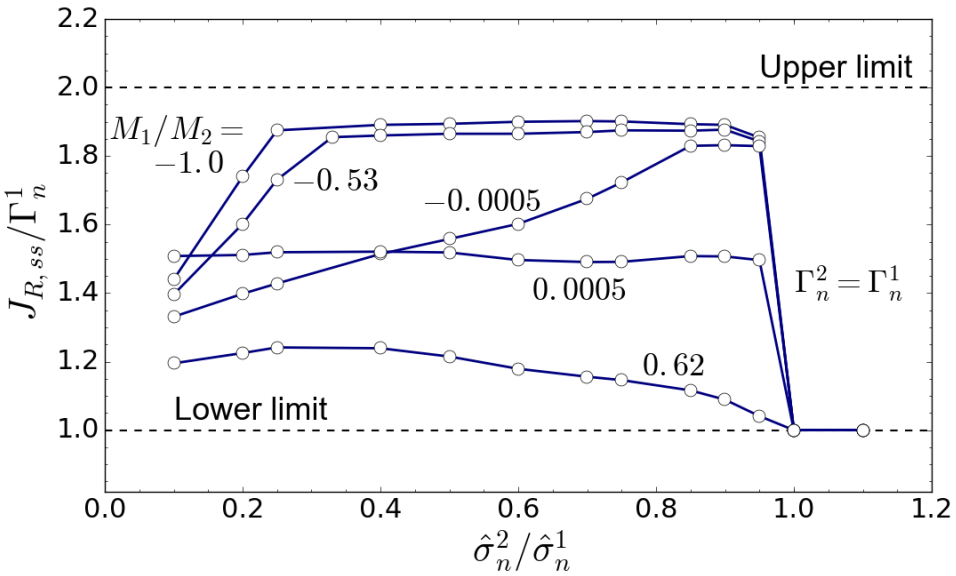

Figure 7: Overall steady-state fracture resistance, $J_{R,ss}$, under mix mode loading, as a function of the normal peak traction of the secondary crack located at a distance $h/H = 0.01$ from the primary crack. Cohesive peak tractions: $\hat{\sigma}_n^1 = \hat{\sigma}_t^1$ and $\hat{\sigma}_n^2 = \hat{\sigma}_t^2$.

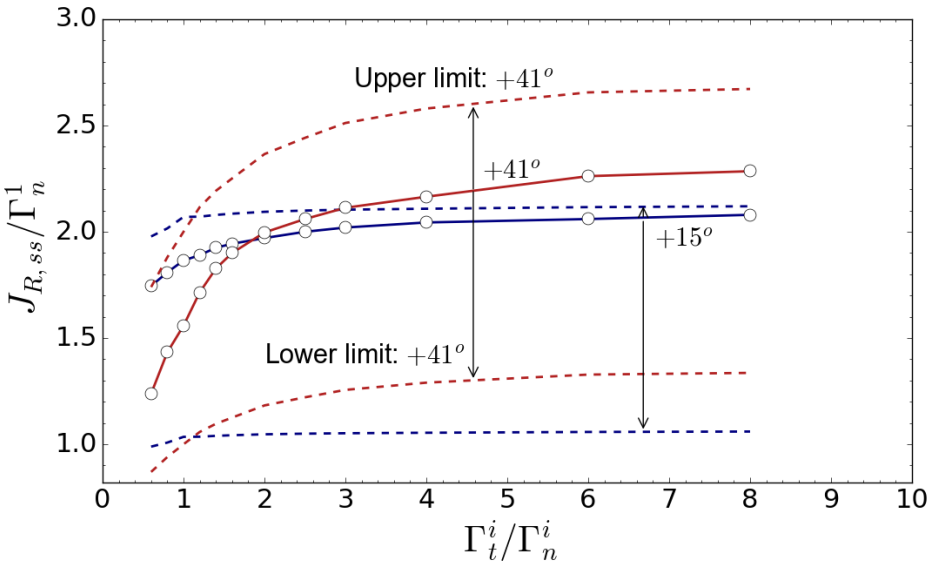

Figure 8: Overall steady-state fracture resistance, $J_{R,ss}$, under mix mode loading, as a function of the fracture energy of the secondary crack located at a distance $h/H = 0.01$ from the primary crack. $\Gamma_t^1 = \Gamma_n^1$, $\Gamma_t^2 = \Gamma_n^2$, $\hat{\sigma}_n^2/\hat{\sigma}_n^1 = 0.5$ and $\hat{\sigma}_t^2/\hat{\sigma}_t^1 = 0.5$.

In Fig. 8, the effect of the mode II fracture energy relative to the mode I fracture energy on the steady-state fracture resistance is shown for two mode mixities. The lower (Eq. 2) and upper limits (Eq. 3) are also included. The lower limit, for each mode mixity and Γ_t^i/Γ_n^i ratio, was numerically calculated from the finite element of Fig. 4 containing only the primary crack. It can be seen that the overall steady-state fracture resistance is closer to the upper limit as the mode II fracture energy increases relative to the mode I fracture energy.

5 DISCUSSION

The mode I results show the importance of the distance *h* between the primary and secondary crack. The overall steady-state fracture resistance approaches its maximum theoretical value only for small *h* values. As *h* increases, $J_{R,ss}$ does not reach the predicted (upper limit). Thus, effective enhancement of the fracture resistance can be realised only if the weak planes are close to the damage prone areas.

Both mode I and mix mode results show that the overall steady-state fracture resistance can approach the upper limit, for certain combination of geometric and cohesive law properties, but it is always lower than the upper limit. It is shown in [15] that under mode I loading, the left hand side of the secondary crack is not fully closed. Initially it opens and then undergoes unloading and then closes. This can explain why, $J_{R,ss}$ is always lower than the upper limit (Eq. 3). As mentioned above, Eq. 3 assumes that the left hand side of the secondary crack is fully closed.

The enhancement of the overall steady-state fracture resistance is less effective as the mode mixity increases (see Fig. 8). It will be interesting to extend the current work with different mixed mode cohesive laws and investigate how the mix mode coupling affects $J_{R,ss}$.

6 CONCLUSIONS

A theoretical model is developed based on *J* integral. It is shown that a linear dependency exist between the number of cracks/fracture process zones and the overall steady-state fracture resistance. Cohesive zone modelling, consisting of a primary and a secondary crack, is used to examine for which cohesive law parameters of the secondary crack the linear dependency is approximately valid. It was found that the overall steady state fracture resistance was almost double for a wide range of cohesive law parameters as long as the secondary crack lies close to the primary crack. Thus, it is feasible to increase the fracture resistance of a layered structure significantly by simply adding weak layers.

ACKNOWLEDGEMENTS

BFS was supported by the Danish Centre for Composite Structures and Materials for Wind Turbines (DCCSM), Grant No. 09-067212 from the Danish Council for Strategic Research.

REFERENCES

[1] R.Y. Kim, S.R. Soni, Experimental and analytical studies on the onset of delamination in laminated composites, Journal of Composite Materials, **18**, 1984, pp.70-80.

[2] K.A. Dransfield, L.K. Jain and Y.W. Mai, On the effects of stitching in CFRPs - I. Mode I delamination toughness, Composites Science and Technology, **58**, 1998, pp. 815-827.

[3] J.K Kim, C. Ballie, J. Poh and Y.W. Mai, Fracture toughness of CFRP with modified epoxy matrices, Composites Science and Technology, 43, 1992, pp. 283-297.

[4] D.W.Y. Dong, L. Lin, P.T. McGrail, T. Peijs and P.J. Hogg. Improved fracture toughness of carbon fibre/epoxy composite laminates using dissolvable thermoplastic fibres, Composites Part A, **41**, 2006, pp. 759-767.

[5] H. Hess and N. Himmel, Structurally stitched NCF CFRP laminates. Part 1: Experimental characterization of in-plane and out-of-plane properties, Composites Science and Technology, **71**, 2011, 549-568.

[6] K.L. Rugg, B.N. Coc and R. Massabo, Mixed mode delamination of polymer composite laminates reinforced through the thickness by z-fibers, Composites Part A, **33**, 2002, 177-190.

[7] D. Falconnet, P.E. Bourban, S. Pandita, J.A.E. Manson and I. Verpoest, Fracture toughness of weft-knitted fabric composites, Composites Part B, **33**, 2002, 579-588.

[8] A.P. Mouritz, C. Baini, I. Herszberg, Mode I interlaminar fracture toughness properties of advanced textile fibreglass composites, Composites Part A, **30**, 1999, 859-870.

[9] M. Rask and B. F. Sørensen, Determination of the J integral for laminated double cantilever beam specimens: The curvature approach, Engineering fracture mechanics, **96**, 2012, pp. 37–48.

[10] S. Feih, J. Wei, P. Kingshott and B.F. Sørensen. The influence of fibre sizing on the strength and fracture toughness of glass fibre composites, Composites Part A, **36**, 2005, 245-255.

[11] B.F. Sørensen, S. Goutianos and T.K. Jacobsen, Strength scaling of adhesive joints in polymer-matrix composites, International Journal of Solids and Structures, **46**, 2009, pp. 741-761.
[12] J.R. Rice, A path independent integral and the approximate analysis of strain concentrations by notches and cracks, Journal of Applied Mechanics, **35**, 1968, pp. 379-386.
[13] D.S. Dugdale, Yielding of steel sheets containing slits, Journal of the Mechanics and Physics of Solids, **8**, 1960, pp.100-104.
[14] G. Barenblatt, The mathematical theory of equilibrium cracks in brittle fracture, Advances in Applied Mechanics, **7**, 1962, pp. 55-129.
[15] S. Goutianos and B.F. Sørensen, Fracture resistance enhancement of layered structures by multiple cracks, Engineering Fracture Mechanics, **151**, 2016, pp. 92-108.
[16] B.F. Sørensen, K. Jørgensen, T.K. Jacobsen and R.C. Østergaard, DCB-specimen loaded with uneven bending moments, International Journal of Fracture, **141**, 2006, pp 163-176.
[17] Q.D. Yang and M.D. Thouless, Mixed-mode fracture analyses of plastically-deforming adhesive joints, International Journal of Fracture, **110**, 2001, pp 175-187.
[18] S. Li, M.D. Thouless, A.M. Waas, J.A. Schroeder and P.D. Zavattieri, Mixed-mode cohesive zone models for fracture of an adhesively bonded polymer matrix composite, Engineering Fracture Mechanics, **73**, 2006, pp. 64-78.